Modeling turbulent reacting methane thermochlorination flows

By A. D. Harvey† AND H. Pitsch

Motivations for and complications involved in modeling turbulent reacting chlorination flows are discussed. A confined turbulent nonpremixed reacting methyl chloride chlorination flow is investigated numerically using large eddy simulation and a Reynolds (Favre-)averaged Navier-Stokes approach with fully coupled chemistry and a detailed multi-step kinetic mechanism. A laminar diffusion flamelet turbulent combustion model is coupled with both the LES and the RANS codes to close the chemical source terms. A RANS solution neglecting chemical source term closure is also obtained. The different calculations are compared, and differences in the solutions are discussed. Computations including the flamelet turbulent combustion model predict a lower peak reaction temperature and a more gradual temperature increase than predictions neglecting closure.

1. Motivations and objectives

Methylene dichloride (M_2), chloroform (M_3), and carbon tetrachloride (M_4) are three basic products of methane chlorination and are produced by high temperature gas phase chlorination of methane or methyl chloride, (M_1). Their primary uses are as industrial solvents, making refrigerants, and the manufacturing of silicon. Methane chlorination reactions proceed by a multi-step series of exothermic reactions which are stabilized in a confined jet configuration where reactants are typically introduced at temperatures well below the minimum activation temperature. Thus, sustained autothermal operation of the device is strongly dependent on the re-circulation of heat furnished by the confined jet design.

As cold incoming gases are heated by re-circulated products, chlorine atom concentration increases exponentially. Eventually a sufficient chlorine radical concentration is attained for the propagation reactions to proceed (producing heat). A portion of the heat is recirculated back into the incoming feed and the remainder is convected out the exit. As the flow in a confined jet reactor whose inlet temperature is sufficiently low is made to increase, in premixed situations the flame speed decreases and the proportion of heat re-circulated will eventually be insufficient to heat the resulting higher volume of incoming fluid to levels capable of sustaining the reaction.

In large scale industrial chlorination devices operated near extinction, complex behaviors have been observed which include low frequency pressure and temperature oscillations and thermoacoustic excitations. This ultimately leads to extinction of the reaction, excessive undesirable by-product formation, or the convection of highly reactive chlorine in downstream equipment ill-suited for this type of exposure. Obviously these outcomes are undesirable, and an important long term goal is to develop an improved understanding of the unstable behaviors which preempts extinction and/or shutdown of

† The Dow Chemical Company, Plaquemine, Louisiana, bharvey@dow.com

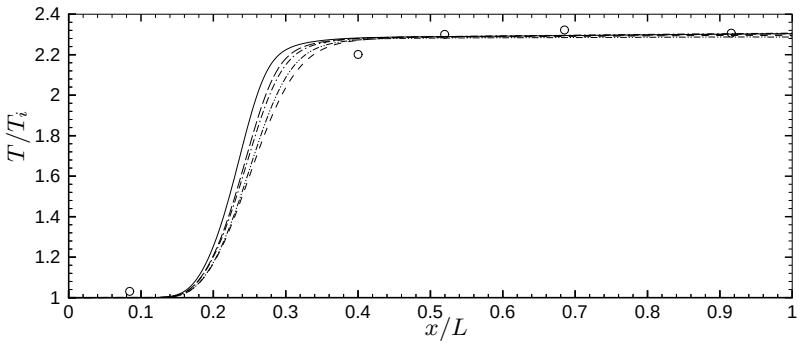

FIGURE 1. Comparison of computed (RANS/no closure) centerline temperature profiles in a commercial scale premixed chloromethanes reactor: ○ - plant data with inflow velocity, $u = 2U_r$; —— $u = U_r$; — — — — $u = 1.5U_r$; —·— $u = 2U_r$; —··— $u = 2.8U_r$; - - - - $u = 4U_r$.

a chloromethanes reactor. In the present study we use a laminar flamelet combustion model, detailed kinetics, and current LES and RANS solution methodologies to study a model nonpremixed methane chlorination device. We discuss combustion modeling issues which will be addressed in ongoing and future studies to ultimately model more realistic chlorination flows. The objectives of this summer research project are:

(*a*) Incorporate a laminar flamelet combustion closure model and detailed, multi-step kinetics into both a chemically reacting RANS code and an LES code.

(*b*) Use the resulting codes to compute the turbulent reacting flow in a nonpremixed methane thermochlorination device.

(*c*) Compare computational results, including the effects of turbulence closure with results obtained with the reacting RANS neglecting closure, and determine the importance of closure modeling for chloromethane chemistry.

1.1. *Past work*

There have been a few documented attempts to model thermal chlorination of methane. West *et al.* (1999) used a 5-step irreversible mechanism in a simple perfectly stirred reactor model that produced dynamical behavior similar to that observed in real reactors operated near the extinction point. Acharya *et al.* (1991) used a second moment closure method in which they assumed fluctuations in temperature and density were small and considered only the correlations $\overline{y''_{M_1} y''_{Cl_2}}$ and $\overline{y''_{M_2} y''_{Cl_2}}$ to model a methane chlorination flow. They conclude that without more detailed kinetics and source term closure, CFD does a poor job of predicting finite-rate chemistry effects, minor species formation, and local reaction extinction. Often, undesirable side reactions, leading to complete decomposition of the products, compete with the main desired chemistry. To study reactor designs and operating conditions which improve selectivity to desirable products, it is important to develop solution strategies capable of handling detailed kinetics. In this study we use a relatively detailed mechanism consisting of 38 species and 152 reactions (Shah & Fox, 1999).

Industrial scale chlorination devices are often more than a meter in diameter and > 10 meters in length with Reynolds numbers exceeding 10^6 at design operation. Three-dimensional velocity fluctuations occur on length scales ranging in sizes equal to this integral scale to a factor of $\mathrm{Re}^{0.75}$ smaller and on a correspondingly broad range of time scales (dynamic range of $\mathrm{Re}^{0.5}$). Relevant chemical time and length scales can be even

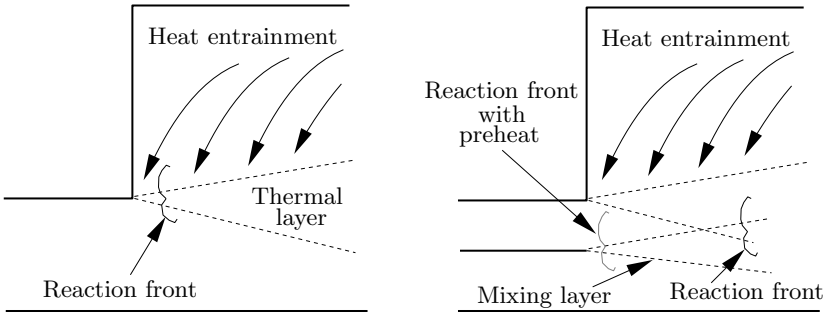

FIGURE 2. Premixed (left) and nonpremixed (right) illustrating the structure of the mixing and reaction front location from preheated and non-preheated feed streams.

broader. Fully resolved LES of such a commercial scale device still remains a considerable computational challenge, and past computational efforts have been restricted to averaged techniques.

Figure 1 compares computed mean temperature profiles for a typical premixed commercial scale reactor with experimental data. Mean temperature measurements were obtained using fixed thermocouples housed in thick thermowells. Due to both the unavailability of optical access and the corrosive environment inside the reactor, measurements on shorter time-scales are difficult to obtain. Axisymmetric calculations were performed at 5 different flow rates, which differ by a factor of 4 using a RANS code including chemical reactions (to be described later) with 15 species and 21 reactions. The chemical source terms in the species equations were evaluated with Favre-averaged values of mass fraction and temperature, neglecting chemical source term closure. The reference velocity is $U_r = 9$ m/s. The data (at the median flow rate) compare reasonably well with the predictions. However, the somewhat limited data suggests a more gradual temperature rise across the reaction zone than the calculations predict. Shah & Fox (1999) did computational studies using a more detailed mechanism and full PDF calculations in an adiabatic, well-stirred device. By varying the mixing time, they show that the increase in temperature is more gradual when the mixing time is longer.

The calculations of Fig. 1 also fail to predict observed sensitivities to variations in flow rates. It is not possible to double (or half) the flow in this particular device without causing undesirable effects such as unsteady pressure oscillations or extinction of the reaction. Computational studies similar to that of Fig. 1, neglecting source term closure and involving variation of other operating parameters such as inlet feed concentration, also fail to predict observed sensitivities in the actual operation of the device.

In the present study we compute the turbulent reacting flow in a chlorination device using detailed kinetics both with and without chemical source term closure, compare differences in solutions, and evaluate the importance of closure.

1.2. *Chlorination modeling difficulties*

Feed streams can typically consist of chlorine, methane, M_1, and M_2 and can be introduced either premixed or nonpremixed through a coaxial configuration with molecular chlorine in one feed entrance and premixed organics in the other. In the present study we investigate the preheated, nonpremixed case; in the future we will look at and report on others. Here we provide a brief description of several inlet configurations to indicate differences in features and reveal relevant modeling issues.

For the premixed case, reaction is initiated and sustained by the confined jet re-

circulation as the cold incoming feed stream is heated (Fig. 2). As flow rates are increased above the flame speed, the reaction front moves farther downstream. The introduction of cold nonpremixed feed can result in a number of complex flame structures. If one of the feed streams is sufficiently heated (typically Cl_2), combustion and flame structure follows that of typical nonpremixed flames. The flame is situated very close to the inlet location, and stable operation is only weakly dependent on the autothermal, confined jet design. However, for cold, nonpremixed applications, flame position and structure are highly dependent on the mixing and heat entrainment processes and can be significantly different depending on which inlet the chlorine is introduced (Raman *et al.*, 2000).

Turbulent reacting flow in chlorination devices can be further complicated by the introduction of liquid chlorine at the inlet (in addition to gas) as a means of increasing chlorine inlet concentration. Thus future combustion modeling of these particular chlorination devices require accounting for the effects of spray vaporization.

In this initial study we use a nonpremixed flamelet combustion model to study a preheated, nonpremixed M_1/M_2 chlorination device. We will couple the combustion model with both LES and Favre-averaged solutions for the flow, turbulence, and scalar mixing. Model characteristics, solution details, and comparisons of computed results are presented next.

2. Solution methodologies

The Favre-averaged Navier-Stokes, LES and Laminar Flamelet codes are briefly described below, referring to available references when possible to conserve space. We use conventional notation, a tilde denoting Favre averaging and an overbar for time-averaged quantities. The ith species partial pressure, density, mass fraction, molecular weight, and enthalpy is p_i, ρ_i, Y_i, W_i, and h_i, and the thermodynamic pressure, mixture density, velocity components, and temperature are given by p, ρ, u, v, w, and T, respectively. Vector quantities are in bold type, and the Favre mean mixture fraction and variance are denoted $\widetilde{Z}$ and $\widetilde{Z''^2}$. Turbulent and laminar diffusivities are denoted by D_t and D_l with constant Schmidt numbers assumed.

2.1. *Reynolds-averaged Navier-Stokes*

A structured, finite-volume, multi-block pressure based low Mach number preconditioned Favre-averaged Navier-Stokes code for a mixture of chemically reacting gases is used. All species are assumed to obey an equation of state: $p_i = \rho_i RT/W_i$. The 3-D equations for n-species partial pressures, momentum, and energy are solved simultaneously in a standard generalized frame of reference. The appropriate vector equation is of the form:

$$\mathbf{\Lambda}\partial_\tau \hat{\mathbf{Q}} + \partial_\xi(\hat{\mathbf{E}} - \hat{\mathbf{E}}_v) + \partial_\eta(\hat{\mathbf{F}} - \hat{\mathbf{F}}_v) + \partial_\zeta(\hat{\mathbf{G}} - \hat{\mathbf{G}}_v) = \hat{\mathbf{H}} \tag{2.1}$$

Where $\hat{\mathbf{Q}}$ is the vector of primitive variables, $\tilde{p}_i$, $\tilde{u}$, $\tilde{v}$, $\tilde{w}$, and $\tilde{T}$. The preconditioning matrix $\mathbf{\Lambda}$ is of a form similar to Choi & Merkle (1993). The hats are used to represent inviscid and viscous flux vectors $\hat{\mathbf{E}}$, $\hat{\mathbf{E}}_v$, etc. in the generalized coordinate system and are related to the flux vectors in the Cartesian frame by an expression of the form

$$\hat{\mathbf{E}} = \frac{1}{J}(\kappa_x \widetilde{\mathbf{E}} + \kappa_y \widetilde{\mathbf{F}} + \kappa_z \widetilde{\mathbf{G}}) \tag{2.2}$$

The mean convective fluxes are differenced using the low-diffusion flux-splitting scheme of Edwards (1997). Flux vectors are linearized and resulting implicit Jacobians, $\partial\hat{G}/\partial\hat{Q}$,

are constructed using derivatives of the fluxes with respect to each of the primitive variables. The exact form of the fluxes and Jacobians can be found in Harvey & Edwards (1998). $\hat{\mathbf{H}}$ contains the chemical production rates per unit volume of each species, $\widetilde{\dot{m}_i}$, which, for calculations neglecting closure, we assume to be equivalent to $\dot{m}_i(\bar{\rho}_i, \widetilde{T})$. Closure of this term is introduced later. The thermodynamic pressure is computed as the sum of partial pressures of each species. Mass fractions are computed from partial pressures, and the enthalpy of each species is computed from

$$h_i = h^{\circ}_{f_i} + \int_{T_r}^{T} C_{p_i} \mathrm{d}T \tag{2.3}$$

where $h^{\circ}_{f_i}$ is the species enthalpy of formation at $T = T_r$ and the species specific heat, C_{p_i}, is obtained using 4th order polynomials in temperature. The mixture-specific heat is obtained by mass fraction weighting.

An arbitrary number of Arrhenius type reactions can be considered. For the present work, the mechanism found in Shah & Fox (1999) is used.

A zonal two-layer k-ϵ model is solved de-coupled from the flow. The eddy viscosity is computed as $C_\mu k^2/\epsilon$. The following transport equations are solved for mean mixture fraction, $\widetilde{Z}$, and variance, $\widetilde{Z''^2}$

$$\bar{\rho}\frac{\partial \widetilde{Z}}{\partial t} + \bar{\rho}\widetilde{\mathbf{u}} \cdot \nabla \widetilde{Z} = \nabla \cdot (D_t \nabla \widetilde{Z}) \tag{2.4}$$

$$\bar{\rho}\frac{\partial \widetilde{Z''^2}}{\partial t} + \bar{\rho}\widetilde{\mathbf{u}} \cdot \nabla \widetilde{Z''^2} = \nabla \cdot (D_t \nabla \widetilde{Z''^2}) + 2\bar{\rho} D_t (\nabla \widetilde{Z})^2 - \bar{\rho}\widetilde{\chi} \tag{2.5}$$

where a gradient transport assumption for turbulent fluxes is used and the mean scalar dissipation rate, $\widetilde{\chi}$, appearing as a sink term in the equation for the mixture fraction variance is calculated as:

$$\widetilde{\chi} = 2\frac{\epsilon}{k}\widetilde{Z''^2} \tag{2.6}$$

The multi-block code employs a multi-level grid refining strategy using three grid levels and is similar to a multigrid V-cycle. Each zone in the grid is solved sequentially using an ILU solver. Additional details can be found in Harvey & Edwards (1998).

2.2. *Large eddy simulation*

The 3-D cylindrical code of Pierce & Moin (1998*b*) is used for the LES calculations. An equation similar to that above for the RANS is solved for the mixture fraction. As in Pitsch & Steiner (2000), the sub-grid scalar mixture fraction variance is expressed as $\widetilde{Z''^2} = C_Z \Delta^2 |\nabla \widetilde{Z}|^2$ with the coefficient, C_Z, determined using the dynamic procedure of Pierce & Moin (1998*a*). Further details of the LES solution techniques and modeling scalar mixing and dissipation rate can be found in these references.

2.3. *Flamelet combustion modeling*

Laminar diffusion flamelet modeling (Peters, 1984; Peters, 2000) has been successfully applied to nonpremixed methane combustion flames in both RANS (Pitsch *et al.*, 1998) and LES (Pitsch & Steiner 2000) frameworks. Following these references the unsteady flamelet equations for the species mass fraction, Y_i, and the temperature are written as

$$\rho\frac{\partial Y_i}{\partial \tau} - \rho\frac{\chi}{2}\frac{\partial^2 Y_i}{\partial Z^2} - \dot{m}_i = 0 \tag{2.7}$$

$$\rho\frac{\partial T}{\partial \tau} - \rho\frac{\chi}{2}\left(\frac{\partial^2 T}{\partial Z^2} + \frac{1}{C_p}\frac{\partial C_p}{\partial Z}\frac{\partial T}{\partial Z}\right) + \frac{1}{C_p}\sum_{k=1}^{N} h_k \dot{m}_k = 0 \tag{2.8}$$

where $\dot{m}_i$ is the chemical production rate per unit volume of species i and the scalar dissipation rate is $\chi = 2D_Z \nabla Z \cdot \nabla Z$ with the diffusion coefficient of the mixture fraction denoted as D_Z. In the so called Lagrangian flamelet model (LFM), flamelets are introduced at the nozzle inlet and are allowed to convect downstream through the flow. An expression which relates the axial position of the flamelet to Lagrangian flamelet time, $\mathrm{d}\tau = \langle \widetilde{u}_{\widetilde{Z}} | \widetilde{Z}_{st} \rangle \mathrm{d}x$, is defined by

$$\tau = \int_0^x \frac{dx'}{\langle \widetilde{u}_{\widetilde{Z}} | \widetilde{Z}_{st} \rangle (x', t)} \tag{2.9}$$

where $\langle \widetilde{u}_{\widetilde{Z}} | \widetilde{Z}_{st} \rangle$ is the resolved velocity component along the mixture fraction contour surface corresponding to the stoichiometric value, $\widetilde{Z}_{st}$. For steady flamelet modeling, the first term on the rhs of (2.7) and (2.8) is zero. Additional derivations and discussions on laminar flamelet equation modeling can be found in Pitsch & Steiner (2000) and Peters (2000).

Solution of Eqs. (2.7)-(2.9) yield the laminar flamelet structure of all scalar quantities $\phi = Y_i$, T. Using an assumed β-function pdf, $\widetilde{P}(Z, \mathbf{x}, t)$, whose shape is determined by the local mean and variance of the mixture fraction, Favre-averaged (RANS) or resolved values (LES) scalar quantities are obtained using

$$\widetilde{\phi}_i = \int_{Z=0}^{1} \phi_i(Z, \mathbf{x}, t) \widetilde{P}(Z, \mathbf{x}, t) dZ \tag{2.10}$$

for all scalars quantities $\phi_i = Y_i$ and T. Note that for RANS calculations, $\widetilde{P}$ denotes the pdf for long time sampling, while for LES, $\widetilde{P}$ is the instantaneous pdf within the filter volume.

The form of the laminar flamelet model described above is not strictly suited to account for regions of strong flow re-circulation and radial diffusion due to the lack of a full description of spatial convection in the flamelet equations. However, for the preheated application to be presented in the next section, the effects of re-circulation is minimized. Application of an extended laminar flamelet concept which incorporates multi-dimensional effects is the subject of a future study.

2.4. *RANS/flamelet model coupling*

Implementation of the steady laminar flamelet (SLF) model entails solving Eqs. (2.7)-(2.10) for all scalar quantities at all possible values of the mean mixture fraction, $0 \leq \widetilde{Z} \leq 1$, variance, $0 \leq \widetilde{Z''^2} \leq 0.25$, and scalar dissipation rate, $0 \leq \widetilde{\chi} \leq \widetilde{\chi}_q$, where $\widetilde{\chi}_q$ is the quenching scalar dissipation rate. A table is then constructed containing $\widetilde{\phi}_i = \widetilde{\phi}_i(\widetilde{Z}, \widetilde{Z''^2}, \widetilde{\chi})$ for the scalars variables $\widetilde{\phi} = \bar{\rho}$, $\widetilde{T}$ and the mixture molecular weight $\widetilde{W}_m$ (required in the RANS implicit Jacobian terms). The flow is solved with the reacting RANS code using a single species equation with a variable molecular weight. At each

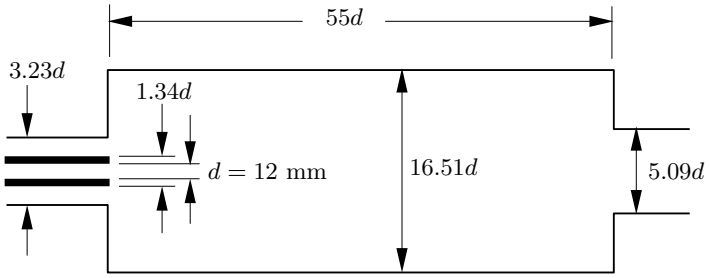

FIGURE 3. Model chloromethanes reactor geometry.

iteration the scalar dissipation rate is obtained from current values of k and ϵ, and $\widetilde{Z}$ and $\widetilde{Z''^2}$ are obtained from Eqs. (2.4) and (2.5), and then reference to the flamelet table is made to obtain new values of the scalar quantities $\bar{\rho}$, $\widetilde{T}$, and $\widetilde{W}_m$. The temperature equation in the RANS code is deactivated, and energy conservation is left to the flamelet code (Eq. 2.8).

In steady flamelet modeling the flamelet time does not appear in the equations, and it is assumed that the scalars, $\widetilde{\phi}$, everywhere in the domain have the same functional dependence $\widetilde{\phi}_i = \widetilde{\phi}_i(\widetilde{Z}, \widetilde{Z''^2}, \widetilde{\chi})$. Once the solution has converged, the mass fractions of each species can be found from a similar flamelet table containing $\widetilde{Y}_i = \widetilde{Y}_i(\widetilde{Z}, \widetilde{Z''^2}, \widetilde{\chi})$.

In the Lagrangian flamelet model (LFM), a different flamelet solution is obtained at each axial plane in the computational grid. Computations incorporating unsteady flamelets involve first obtaining a converged steady flamelet solution to the flow as described above. The velocity of the stoichiometric surface, $\langle \widetilde{u}_{\widetilde{Z}} | \widetilde{Z}_{st} \rangle(x)$, and conditional mean scalar dissipation rate at each plane $\langle \widetilde{\chi} | \widetilde{Z}_{st} \rangle(x)$ are computed in the RANS code. Equations (2.7)-(2.10) are solved for all scalar quantities in all $\widetilde{Z}$ and $\widetilde{Z''^2}$-space, and an unsteady flame table is constructed containing $\widetilde{\phi}_i = \widetilde{\phi}_i(\widetilde{Z}, \widetilde{Z''^2}, x)$ for $\widetilde{\phi} = \bar{\rho}$, $\widetilde{T}$, and $\widetilde{W}_m$. This table is used by the RANS until the mixture field adjusts, at which time a new LFM table is constructed. This whole process is repeated until convergence.

The main implementation difference between SLF and LFM is that $\widetilde{\chi}$ in the SLF table is replaced by the axial coordinate in the LFM table. Each axial coordinate is treated as a separate flamelet with Lagrangian flamelet time given by Eq. (2.9) and with a unique conditionally averaged scalar dissipation rate.

2.5. *LES/flamelet model coupling*

Coupling of the LES calculations and the flamelet model proceeds in much the same manner as the coupling for the RANS. The major difference is in the way the conditional averages, scalar dissipation rate, and mixture fraction variance are computed. Further details can be found in Pitsch & Steiner (2000).

3. Results and discussion

A model nonpremixed chlorination flow is constructed by considering a confined coaxial jet configuration with inner pipe diameter, d (see Fig. 3). The use of subscripts p and a will denote quantities in the inner pipe and annulus, respectively. Chlorine preheated to T_p =800K is introduced through the inner jet and premixed M_1 ($Y_{M_1} = 0.47$) and M_2 ($Y_{M_2} = 0.53$) at T_a =323K is introduced through the annulus. The velocity ratio is

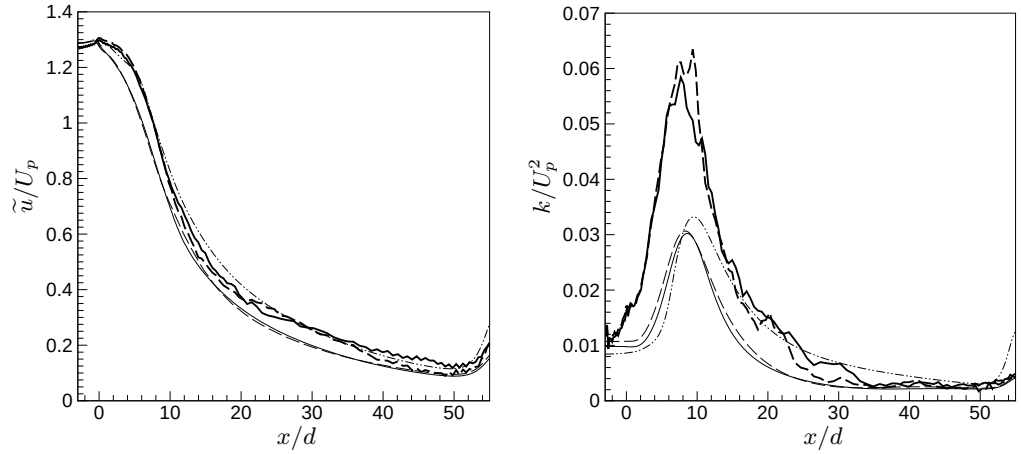

FIGURE 4. Centerline mean axial velocity (left) and kinetic energy profiles (right); ——— LES/LFM; - - - - LES/SLF; ——— RANS/LFM; - - - - RANS/SLF; —··— RANS/NC.

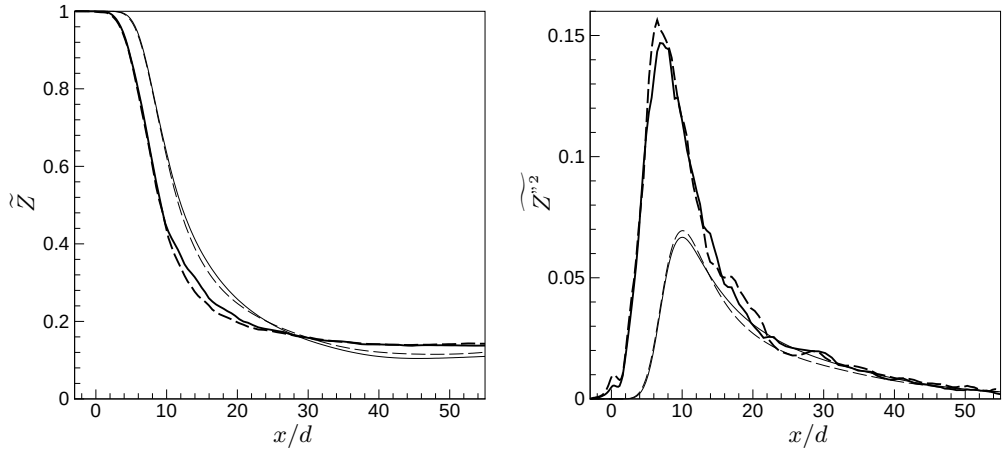

FIGURE 5. Centerline mean mixture fraction (left) and mixture fraction variance (right); ——— LES/LFM; - - - - LES/SLF; ——— RANS/LFM; - - - - RANS/SLF.

$U_p/U_a = 5$, the total Cl_2 mass fraction is 24%, and the bulk inner pipe velocity, U_p, is 7.905 m/s ($Re_p = 11910$). In all the RANS and LES calculations, fully developed turbulent profiles were computed using an appropriately long coaxial pipe. LES calculations were performed on a $130 \times 50 \times 24$ grid. For the present RANS work, 2-D axisymmetric calculations were carried out on a 6-zone grid with a total combined resolution of 225×129.

Computed centerline mean velocity and turbulent kinetic energy profiles are shown in Fig. 4 for all calculations. Predictions of velocity decay rates are similar for both RANS and LES. Mean velocity for the RANS calculations with flamelet combustion modeling drop off faster near the inlet, primarily due to the delay in the rise of kinetic energy near the entrance compared to the LES computations. LES predictions of kinetic energy showed a spike at the centerline which could possibly be an artifact of the boundary

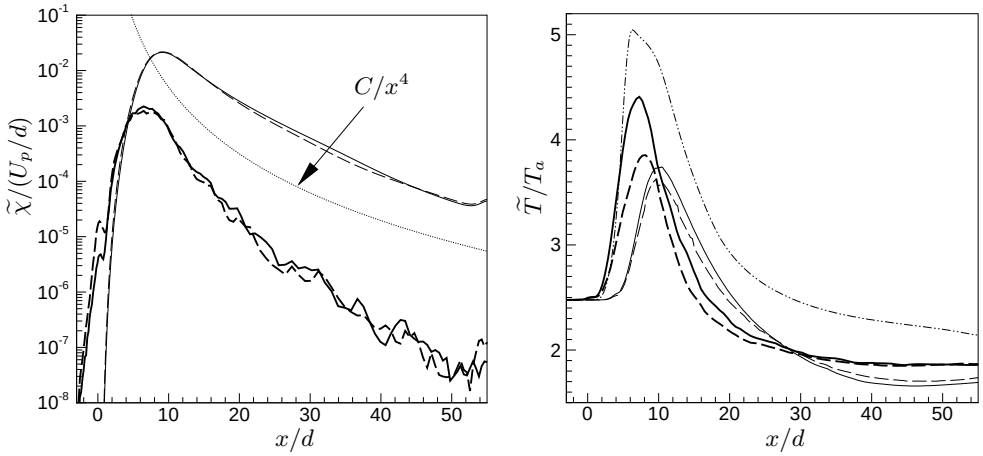

FIGURE 6. Centerline mean scalar dissipation rate (left) and mean temperature (right); ——— LES/LFM; - - - - LES/SLF; ——— RANS/LFM; - - - - RANS/SLF; —·—·— RANS/NC.

treatment and is currently being investigated further. The RANS computation neglecting closure closely follows the LES predictions of centerline velocity. This is because the temperature (shown later) is higher near the entrance than all other calculations, further resulting in an increased velocity compared to the other RANS calculations and offsetting the effect due to the lower kinetic energy levels seen in the LES.

Mean mixture fraction and mixture fraction variance are shown in Fig 5. Decay rates of $\widetilde{Z}$ are similar for the LES and RANS calculations. Unlike the velocity, which falls off quicker near the entrance for the RANS, the LES predicts a more rapid drop in $\widetilde{Z}$ at the nonpremixed nozzle exit. Differences between predicted centerline decay rates and overall levels of $\widetilde{Z}$ and $\widetilde{Z''^2}$ using the steady and unsteady flamelet model (SLF vs. LFM) are small.

Computed scalar dissipation rate along the centerline is shown in Fig. 6. RANS predictions are much higher than the LES calculations. Both techniques, however, predict similar decay rates that compare reasonably well with an C/x^4 scaling for an arbitrary constant C (dotted line).

Centerline temperature profiles are shown on the right of Fig. 6. Peak temperatures are highest and the temperature increase is steepest for the calculations neglecting closure. The significantly higher temperature predicted by the RANS calculation neglecting closure can be partially attributed to the fact that this is the only calculation performed in this study that takes into full account the effects of the flow re-circulation in the energy equation. The Lagrangian flamelet model (LFM) predicts higher peak temperatures and a faster temperature increase in the reaction zone than the steady flamelet model (SLF) results. The differences in the flow and mixing results are negligible.

Figure 7 shows differences in the computed mean velocity fields for the LES calculations (upper) and RANS (lower) coupled with the unsteady flamelet model. Results compare well; the largest discrepancies appear to be closest to the centerline.

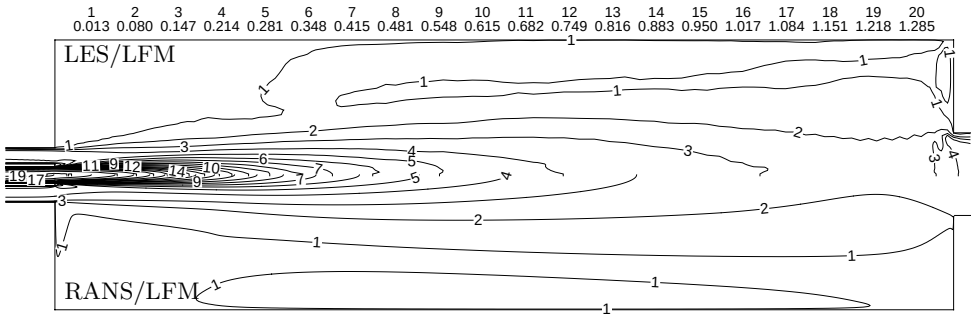

FIGURE 7. Comparison of mean velocity, $\widetilde{u}/U_p$; LES/LFM (upper); RANS/LFM (lower).

4. Conclusions

Issues associated with modeling gas phase reacting methane thermochlorination flows in the petrochemical industry have been discussed. Commercial scale devices can be very large, and accurate model development and application must ultimately take into account both nonpremixed and premixed combustion physics with spray evaporation. RANS modeling neglecting turbulence closure fails to predict finite-rate chemistry effects, intermediate species formation, and localized reaction extinction.

A laminar diffusion flamelet combustion model was successfully coupled with a RANS code and a CTR-developed LES code. The turbulent reacting flow in a preheated, nonpremixed methyl chloride thermochlorination device was computed. The largest differences between the RANS and LES computational results are in the predictions of the turbulent kinetic energy and scalar mixing. LES predictions of turbulent kinetic energy are significantly higher than the RANS calculations. Naturally one suspects the LES methodology to fare better in this regard. The differences in the centerline kinetic energy between the RANS and LES results are being examined further.

All calculations using the laminar flamelet closure predict lower peak temperatures in the reaction zone than the fully coupled reacting RANS calculation-neglecting closure. Use of the flamelet combustion model results in a more gradual increase in temperature in the reaction zone and possibly indicates that inclusion of source term closure results in a slower reaction rate compared to computations-neglecting closure. It could also be possible that the steeper gradient in the calculations-neglecting closure results because a higher maximum temperature must be reached at a comparable flame location.

Related ongoing work in support of this effort includes further investigations into nonpremixed turbulent chlorination flows. This work includes using an extended flamelet model which accounts for multi-directional diffusion effects between neighboring flamelets as well as the solution of a G-equation coupled with a flamelet model for premixed chlorination applications. These computational techniques should bring us closer to the longer term goal of developing methods for predicting complex combustion phenomena such as lifted flames, localized extinction, and re-ignition in thermochlorination devices.

Acknowledgments

The authors thank the management of Hydrocarbons Research at Dow Chemical for providing financial support and the staff, coordinators, and visiting researchers at CTR

for providing a stimulating research environment in which this work took place. In particular, Professor Parviz Moin for providing the opportunity to participate and Dr. Chong Cha and Professor Dan Haworth for many educational discussions on turbulent combustion modeling.

REFERENCES

Acharya, S., Jang, D. S., West, D. H. & Hebert, L. A. 1991 A moment closure method for modeling a multistep chlorination reaction. *AIChE Paper 33a*, AIChE Spring National Meeting, Houston TX.

Choi, Y. & Merkle, C., L. 1993 The application of preconditioning in viscous flows. *J. Comp. Phys.* **105**, 207-223.

Edwards, J. R. 1997 A low-diffusion flux-splitting scheme for Navier-Stokes calculations. *Computers & Fluids.* **26**, 645-659.

Harvey, A. D. & Edwards, J. R. 1998 Preconditioned Navier-Stokes for laminar methane-air nonpremixed combustion. (Unpublished), presented at American/Japanese Flame Research Committee International Symposium, Maui Hawaii.

Peters, N. 1984 Laminar diffusion flamelet models in nonpremixed turbulent combustion. *Prog. Energy Combust. Sci.* **10**, 319-339.

Peters, N. 2000 Turbulent Combustion, Cambridge University Press.

Pierce, C. D., & Moin, P. 1998*a* A dynamic model for subgrid-scale variance and dissipation rate of a conserved scalar. *Phys. Fluids.* **10**, 3041-44.

Pierce, C. D., & Moin, P. 1998*b* Large eddy simulation of a confined coaxial jet with swirl and heat release. AIAA Paper 98–1892.

Pitsch, H., Chen, M. & Peters, N. 1998 Unsteady flamelet modeling of turbulent hydrogen/air diffusion flames. *Twenty-seventh Symposium (Int.) on Combustion*, The Combustion Institute, 1057-1064.

Pitsch, H. & Steiner, H. 2000 Large-eddy simulation of a turbulent piloted methane/air diffusion flame (Sandia flame D). *Phys. Fluids.* **12**, to appear.

Raman, V., Fox, R. O., & Harvey, A. D. 2000 Full PDF simulation of a coaxial thermochlorination reactor. *Paper JL.005,* 53rd APS Annual Meeting of DFD, Washington, DC.

Shah, J. J. & Fox, R. O. 1999 CFD simulation of chemical reactors: application of in situ adaptive tabulation to methane thermochlorination chemistry. *Ind. Eng. Chem. Res.* **38**, 4200-12.

West, D. H., Hebert, L. A. & Pividal, K. A. 1999 Detection of quenching and instability in industrial chlorination reactors. *AIChE Paper 4b,* AIChE Fall National Meeting, Miami FL.